Received: 19 May 2021 | Revised: 15 June 2021 | Accepted: 5 July 2021

DOI: 10.1002/nano.202100194

RESEARCH ARTICLE

A facile method for synthesizing polymeric nanofiber-fragments

Aihik Banerjee[1] | **Tanvi Jariwala**[1] | **Sanggon Kim**[1] | **Youyi Tai**[1] | **Sharon Chiang**[1] | **Honghyun Park**[2] | **Nosang V. Myung**[3] | **Jin Nam**[1]

[1] Department of Bioengineering, University of California-Riverside, Riverside, California 92521, USA

[2] Korea Institute of Materials Science, 797 Changwondaero, Seongsan gu, Changwon, Gyeongnam, South Korea

[3] Department of Chemical and Biomolecular Engineering, University of Notre Dame, Notre Dame, Indiana 46556, USA

Correspondence
Jin Nam, Department of Bioengineering, University of California, Riverside, Riverside, CA 92521, USA.
Email: jnam@engr.ucr.edu

Aihik Banerjee and Tanvi Jariwala contributed equally to this study.

Funding information
National Science Foundation, Grant/Award Number: CBET-1805975; National Research Foundation of Korea; Ministry of Science and ICT, Grant/Award Number: 2018M3D1A1057844; UC Riverside and Korea Institute of Materials Science, Grant/Award Number: PNK7280

Abstract

Electrospinning is a versatile method for synthesizing nanofibrous structures from nearly all polymers, offering a solution for the industrial-scale mass production of nanomaterials in a wide range of applications. However, the continuous non-woven structure intrinsic to electrospun fibers limits their applications, where a smaller length scale is desired. Here, we present a novel method to synthesize polymeric nanofiber-fragments based on colloid electrospinning of polymer and sacrificial silica nanoparticles, followed by mechanical fracturing with ultrasonication. The size and hydrophobicity of silica nanoparticles are optimized for their improved integration within the polymer matrix, and the controllability of nanofiber-fragment length by the amount of silica nanoparticle loading, down to 2 μm in length for poly(vinylidene fluoride-trifluoroethylene) nanofibers with an average fiber diameter of approximately 100 nm, is shown. The resultant nanofiber-fragments are shown to maintain their material properties including piezoelectric coefficients and their enhanced injectability for drug delivery application is demonstrated with an animal model.

KEYWORDS
electrospinning, fragmentation, nanofiber, piezoelectric

1 | INTRODUCTION

The dimensional scale of materials significantly influences their functionality including interaction with living organisms such as cellular responses, biomembrane transport, circulation within the body, and their excretion.[1–3] Such dimensional dependency often limits the bio-applications of a material. For example, an important factor in employing a polymeric material for a drug delivery system is the degradation/removal of the material after drug release. Traditionally, naturally derived polymers or synthetic biodegradable polymers have been primarily used because they can be enzymatically degraded and directly excreted from the body via the renal system. For such a selection of materials, however, there is a limitation in manipulating their physicochemical properties to enhance drug

release efficacy and/or precisely control drug release kinetics.[4–6] In this regard, functional materials, albeit non-biodegradable, present alternative opportunities to exploit their structural and chemical characteristics tailored for specific drug delivery applications, that is, stimuli-responsive controlled drug release.[7–8] The major drawback of non-biodegradable polymeric nanofibers is that they need to be surgically removed after drug release, limiting their applications in deep tissue implantation. The excretion of synthetic non-biodegradable polymers in vivo depends on its interaction with liver cells, mainly endothelial cells and Kupffer cells.[9] These cells play a major role in clearing foreign materials from the systemic circulation for relatively small-sized foreign materials (~7 μm).[10] Therefore, the development of optimal nano/micro-sized drug carriers that can be easily removed by the renal system while providing a sufficient payload with a specific functionality has been an area of focus to enhance biocompatibility and drug delivery efficacy.

Several methods have been developed to synthesize nanoparticles or nanofragments. Especially, nanorods or nano-whiskers having a high aspect ratio are more advantageous for drug delivery applications due to their anisotropy enhancing passive diffusion across the plasma membrane for effective phagocytosis.[1] Nano-whiskers, elongated rod-like crystals with a dimension of 10–1000 nm in length, have been synthesized using several different methods.[11] These methods typically involve either breaking down of large size into small particles or building up from seed via crystal growth. For example, cellulose nano-whiskers of 200–250 nm in length can be synthesized using acid hydrolysis[12] while metal nano-whiskers of 1 μm length can be synthesized using high-temperature glancing angle deposition.[13] These methods, however, cannot be applied to organic materials without hydrolyzable chemical bonds. On the other hand, the nanotemplate-mediated synthesis approach provides a means to control the exact dimensions of nanoparticles, but it is limited in its ability for mass production and its applicability for diverse types of polymers.[14]

Electrospinning is a highly versatile method for synthesizing nanoscale fibers nearly from any polymers and polymer blends, offering a wide range of applications in a variety of fields from energy, environment to healthcare.[8,15–17] It produces ultrathin fibers with a large surface area with ease of nanofiber functionalization for therapeutic applications.[18] Combining this with the simplicity of the process for large-scale production makes electrospinning a very attractive method for drug delivery applications. Indeed, we have recently demonstrated that the enhanced piezoelectric properties of electrospun poly(vinylidene fluoride-trifluoroethylene) (P(VDF-TrFE)) nanofibers can be exploited for on-demand, spatiotemporally controlled drug release.[8] However, long, continuous fibers from electrospinning are not excretable as they are too large for phagocytosis by Kupffer cells. Numerous techniques, such as grinding,[19] cutting,[20] ultrasonication,[21] and homogenizers,[22] have been utilized in attempts to fragment electrospun nanofibers. Ultrasonication is reported to be the most efficient method in terms of simplicity and uniformity, however, its utility is limited to highly brittle polymers.[21]

In this study, we aimed to develop a facile method for producing uniform-sized fragments from electrospun nanofibers, universally applicable for various polymers regardless of their mechanical properties. We utilized the colloid electrospinning of polymer and sacrificial nanoparticles to create a beads-on-a-string structure and subsequent chemical removal of the nanoparticles to introduce mechanical weak points along the fibers. These mechanically weak, stress points were exploited by ultrasonication for efficient fracturing of otherwise ductile polymer nanofibers, applicable for a wide range of polymers. The Ströber method was utilized to synthesize various sized silica nanoparticles and the effects of their surface modifications on the integration of nanoparticles in the polymer matrix in order to efficiently fragment the nanofibers were investigated. The controllability of fragment length by varying the silicon dioxide (SiO_2) loading on electrospun nanofibers and its applicability to polymers having distinct mechanical properties were determined, demonstrating the universal practicality in producing polymeric nanofiber fragments.

2 | RESULT AND DISCUSSION

The proposed fragmentation method of electrospun nanofibers is based on using colloid electrospinning for the incorporation of sacrificial ceramic nanoparticles into individual nanofibers and their subsequent chemical removal to create brittle points along the nanofibers (Figure 1). Applied mechanical forces via ultrasonication would then fracture the nanofibers near these brittle points under a temperature below the polymer's glass transition temperature. The keys for this scheme include 1) the size of nanoparticle that is small enough to allow colloid electrospinning, but large enough to create weak junctions along the nanofiber, 2) the surface characteristics of nanoparticles that allow integration of the particles within the nanofiber, and 3) the amount of nanoparticle loading that controls the inter-nanoparticle distance along individual nanofibers; thus, the length of nanofiber-fragments. Therefore, the size and chemical compatibility of the embedded nanoparticles to the host nanofibers is crucial for full integration, making the

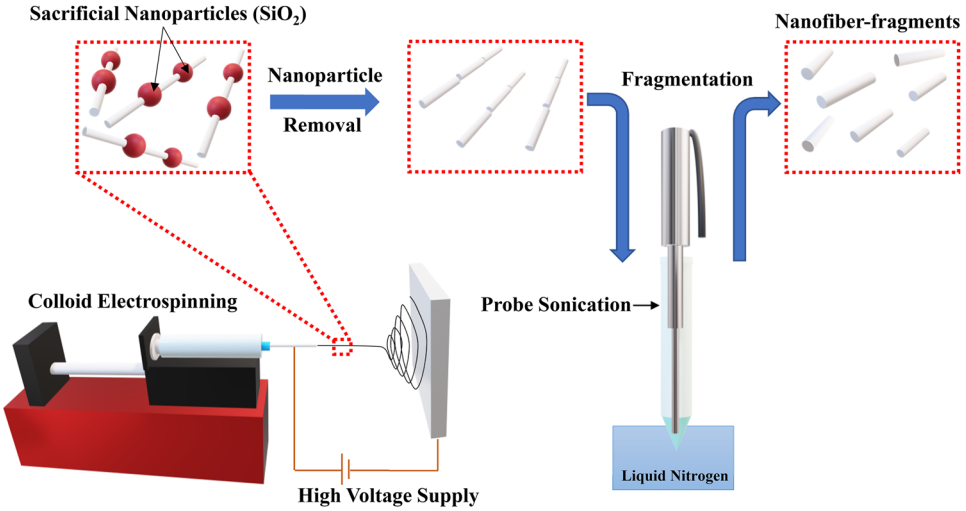

FIGURE 1 Schematic illustration of nanofiber-fragment synthesis. Colloid electrospinning is used to synthesize nanofibers embedded with sacrificial SiO_2 nanoparticles. As-spun nanofibers are subjected to chemical removal of SiO_2 nanoparticles, followed by ultrasonication at low temperature in a liquid nitrogen bath for fragmentation

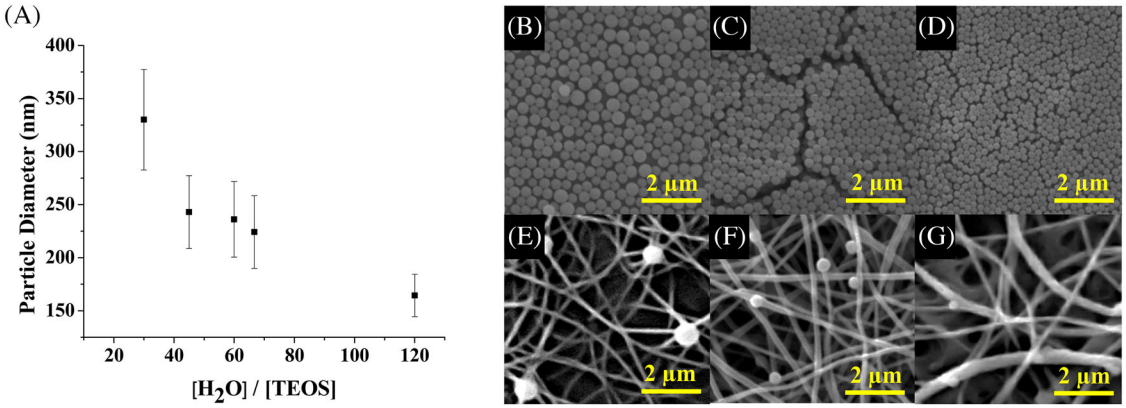

FIGURE 2 The effects of SiO_2 nanoparticle size on their incorporation into electrospun poly(vinylidene fluoride-trifluoroethylene) (P(VDF-TrFE)) nanofibers. (A) Average diameter of SiO_2 nanoparticles as a function of $[H_2O]/[TEOS]$ mole ratio. (B-D) SEM images of approximately (A) 30, (B) 60, and (C) 120 $[H_2O]/[TEOS]$ mole ratios resulting in SiO_2 nanoparticles having average particle diameters of approximately 350, 250, and 150 nm, respectively. (E-G) SEM images of electrospun P(VDF-TrFE) nanofibers embedded with (E) 350, (F) 250, and (G) 150 nm SiO_2 nanoparticles (scale bar = 2 µm)

edges of polymer-nanoparticle interface necking points under mechanical perturbation after the removal of nanoparticles, thus, enhancing the fragmentation of the nanofibers.

2.1 | Optimization of SiO_2 nanoparticle size and surface hydrophobicity for colloid electrospinning

In order to determine the optimal reaction conditions for the synthesis of homogeneous and monodispersed SiO_2 nanoparticles, the effect of [water]/[tetraethyl orthosilicate] ($[H_2O]/[TEOS]$) mole ratio on particle size was investigated (Figure 2A-D). With increasing the ratio, the particle size decreased along with size variation to form monodispersed SiO_2 nanoparticles. SiO_2 nanoparticles having three representative particle sizes of approximately 350, 250, and 150 nm, produced from $[H_2O]/[TEOS]$ ratio of 30, 60, and 120, respectively, were incorporated into P(VDF-TrFE) electrospinning with 5 wt.% nanoparticle loading (Figure 2E-G). The larger particle size exhibited poor integration within the nanofiber and resulted in the formation of nodes involving multiple nanofibers while SiO_2 nanoparticles with the smaller particle size were either completely embedded within nanofibers or

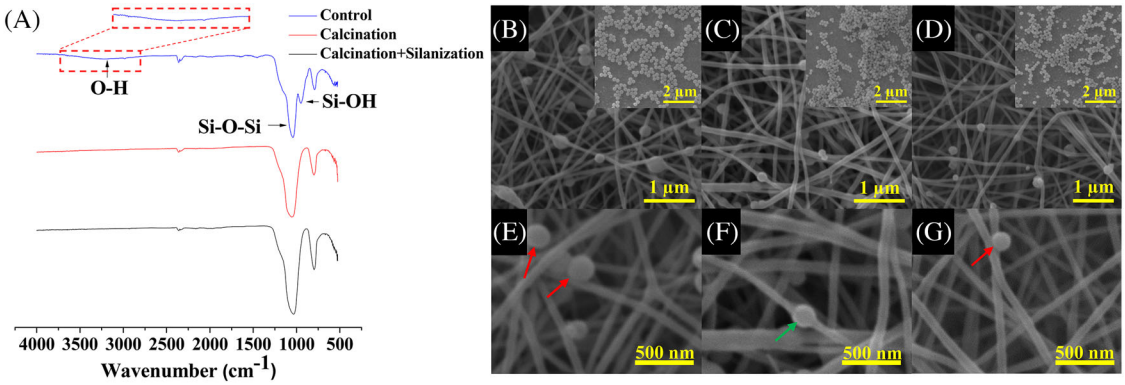

FIGURE 3 FTIR characterization of SiO_2 nanoparticles with various surface modifications and its effects on particle incorporation into poly(vinylidene fluoride-trifluoroethylene) (P(VDF-TrFE)) nanofibers. (A) FTIR spectra comparing hydrophilic (O-H and Si-OH) and hydrophobic (Si-O-Si) peaks among SiO_2 nanoparticles with no modification (control), calcination, and silanization in addition to calcination. (B-G) SEM images of electrospun P(VDF-TrFE) nanofibers embedded with (B, E) as-synthesized SiO_2 nanoparticles or those subjected to post-processing for enhanced hydrophobicity by (C, F) calcination at 900°C for 3 hours or (D, G) calcination followed by surface silanization (insets show SiO_2 nanoparticle morphologies after each surface modification without any noticeable changes). Red arrows indicate SiO_2 nanoparticles attached mostly on the surface of P(VDF-TrFE) nanofibers while green arrow indicates SiO_2 nanoparticle embedded in the body of the nanofibers (scale bar = 500 nm)

surface attached. Therefore, SiO_2 nanoparticles with an average diameter of approximately 250 nm, which was more than two-fold larger than the nanofiber size, yet uniformly integrated into individual nanofibers, were utilized in the subsequent experiments.

Since the degree of SiO_2 nanoparticle integration in individual nanofibers, that is, surface decoration versus full-body embedment, is critical for creating uniform defects in the nanofibers, the physical interaction between SiO_2 nanoparticles and P(VDF-TrFE) nanofibers was optimized to promote complete embedment of the nanoparticles into the nanofibers. SiO_2 nanoparticles of approximately 250 nm in diameter with three types of surface modifications—as-synthesized (control), calcination, and calcination followed by silanization—were prepared and characterized using Fourier-transform infrared spectroscopy (FTIR) (Figure 3A). The control as-synthesized SiO_2 nanoparticles without post-modification exhibited transmittance peaks approximately at 800 and 3400 cm^{-1}, which are attributed to the hydroxide group, indicating a certain degree of hydrophilicity.[23] These characteristic peaks were removed by both calcination and calcination-silanization, increasing hydrophobicity. Furthermore, the calcined SiO_2 nanoparticles with subsequent silanization exhibited the strongest peak associated with siloxane (Si-O-Si) at approximately 1000 cm^{-1}, indicating the greatest hydrophobicity.

Each type of SiO_2 nanoparticle with different surface modifications was electrospun with P(VDF-TrFE) to synthesize nanocomposite fibrous membrane (Figure 3B-D). All conditions showed a beads-on-a-string morphology. However, a closer examination revealed that the calcined nanoparticles were well-integrated within the nanofibers as compared to as-synthesized and calcined-silanized SiO_2 nanoparticle conditions, where the nanoparticles were attached to the surface of the nanofibers (Figure 3E-G). The relatively hydrophilic nature of as-synthesized nanoparticles due to the hydroxide groups present on the surface resulted in failing the complete integration of the nanoparticles within the center of the nanofibers of a hydrophobic polymer, P(VDF-TrFE). Similarly, the nanoparticles with silanization exhibited superhydrophobicity, failing to match the properties of the precursor polymer solution, required for full integration. In contrast, the calcined nanoparticles were compatible with the hydrophobicity properties of the precursor solutions to produce efficient integration within the nanofibers, suggesting the importance of regulating nanoparticle surface chemistry compatible with electrospinning precursor solutions. As such, aqueous electrospinning systems would be compatible with hydrophilic as-synthesized SiO_2 nanoparticles.

2.2 | Fragmentation of SiO_2 embedded-nanofibers

To demonstrate controllability of nanofiber-fragment length, P(VDF-TrFE) nanofibers embedded with various concentrations of calcined SiO_2 nanoparticles including 0, 10, 20, 40, or 60 wt.% loading were synthesized and characterized. The nanoparticles of approximately 250 nm in diameter were utilized for colloid electrospinning (Figure 4A). As compared to control nanofibers without

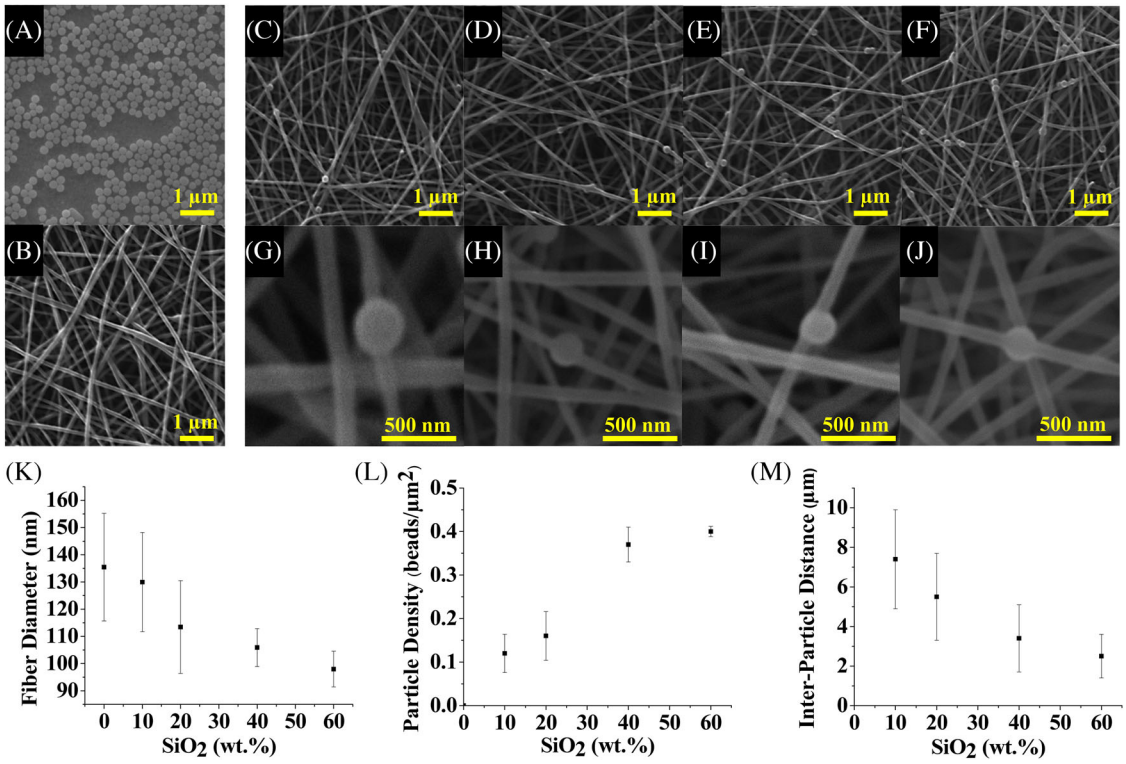

FIGURE 4 Morphological characterization of electrospun poly(vinylidene fluoride-trifluoroethylene) (P(VDF-TrFE)) nanofibers embedded with various SiO_2 nanoparticle loadings and their resultant nanofiber-fragments. (A-B) SEM images of (A) calcined SiO_2 nanoparticles (scale bar = 1 μm), (B) electrospun P(VDF-TrFE) nanofibers without SiO_2 nanoparticles (scale bar = 1 μm). (C-J) SEM images of electrospun P(VDF-TrFE) nanofibers with (C, G) 10, (D, H) 20, (E, I) 40 and (F, J) 60 wt.% SiO_2 nanoparticles showing no significant change in fiber morphology and well-integrated nanoparticles with the polymer nanofibers, independent of nanoparticle density. (K-M) The effects of SiO_2 nanoparticle loading on (K) P(VDF-TrFE) fiber diameter, (L) SiO_2 nanoparticle density within nanofiber matrix, and (M) inter-particle distance on an individual nanofiber

SiO_2 nanoparticles (Figure 4B), all conditions exhibited the typical cylindrical shape of electrospun nanofibers (Figure 4C-F). Closer examination showed that the nanoparticles were well-integrated within the body of nanofibers in all conditions (Figure 4G-J). The resulting fiber diameter, SiO_2 particle density, and inter-particle distance on an individual fiber were compared as a function of SiO_2 loading (Figure 4K-M). With the increase of SiO_2 loading, the P(VDF-TrFE) nanofiber diameter proportionally decreased (Figure 4K). This decrease in nanofiber diameter may result from an increase in the electrospinning solution conductivity due to SiO_2 nanoparticle loading.[24–25] As expected, the particle density within the nanofibrous membrane increased as SiO_2 loading increased (Figure 4L), and as a result, the inter-particle distance between two nanoparticles along an individual nanofiber decreased (Figure 4M).

These SiO_2 nanoparticle-embedded P(VDF-TrFE) nanofibers were subjected to hot mild alkaline treatment to remove the SiO_2 nanoparticles, introducing brittle points along the nanofibers (Figure 5A-C). The nanofiber membrane was then immersed in a water bath and a liquid nitrogen bath for 30 minutes each, followed by ultrasonication. The nanofiber-fragments were subsequently isolated by ultracentrifugation (Figure 5D-H). As compared to the control sample where the microstructure of the nanofibrous membrane was intact after mechanical perturbation using high power sonication, the nanofibers were fragmented with their length decreasing as the nanoparticle loading increased. The length of nanofiber-fragments was closely related to the interparticle distance in as-synthesized composite nanofibers, clearly demonstrating the controllability of this method to produce nanofiber-fragments with the desired length (Figure 5I). Therefore, our novel fragmentation method provides a means to balance the size of nanofiber-fragments for injectability/biocompatibility and process efficiency.

To demonstrate the universal applicability of this fragmentation method, poly(ε-caprolactone) (PCL) nanofibers, one of the softest polymers that are extensively used in biomedical applications, were synthesized with and without SiO_2 nanoparticles and subjected to fragmentation. P(VDF-TrFE) nanofibers at this diameter range having a single fiber elastic modulus of approximately

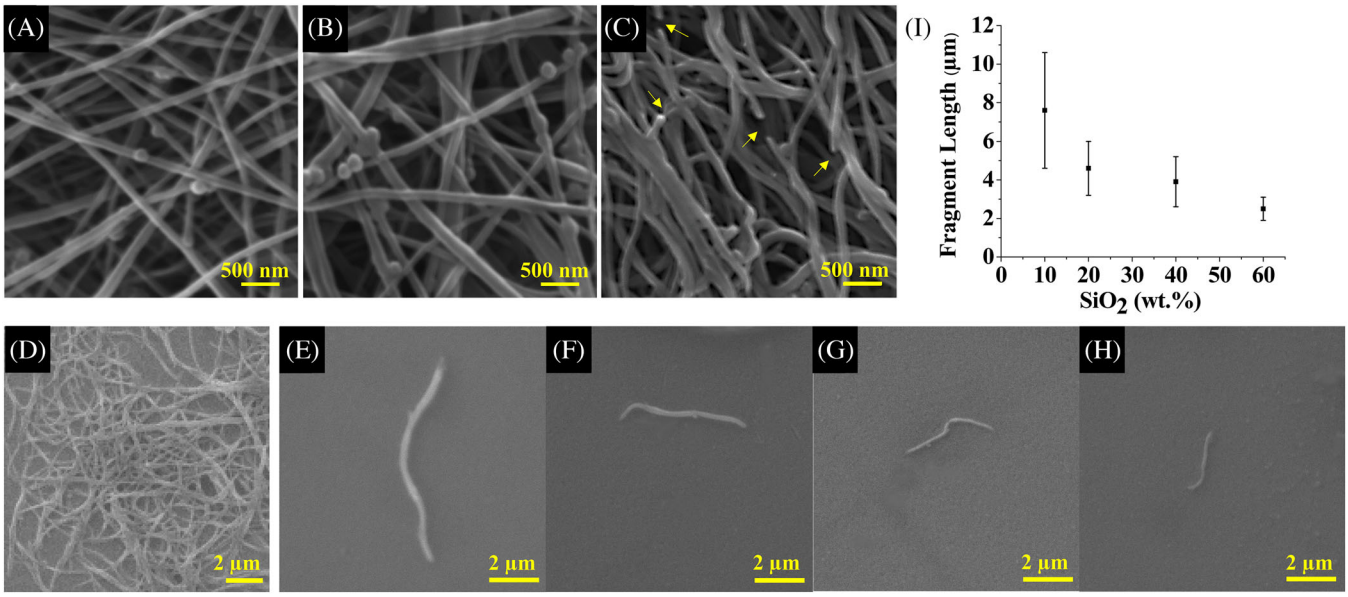

FIGURE 5 Morphological characterization of electrospun poly(vinylidene fluoride-trifluoroethylene) (P(VDF-TrFE)) nanofibers with SiO_2 nanoparticle integration and subjected to hot mild alkaline treatment. SEM images of as-spun P(VDF-TrFE) nanofibers with 20 wt.% SiO_2 nanoparticles (A) before, and after treatment with (B) DI water (control), and (C) 0.2 M KOH, at a temperature of 70°C for 90 minutes. Arrows indicate defects created by the SiO_2 nanoparticle removal. (D-H) SEM images of nanofiber-fragments produced by chemical treatment and ultrasonication of P(VDF-TrFE) nanofibers embedded with (D) 0, (E) 10, (F) 20, (G) 40, and (H) 60 wt.% SiO_2 nanoparticles. (I) P(VDF-TrFE) nanofiber-fragment length as a function of SiO_2 nanoparticle loading

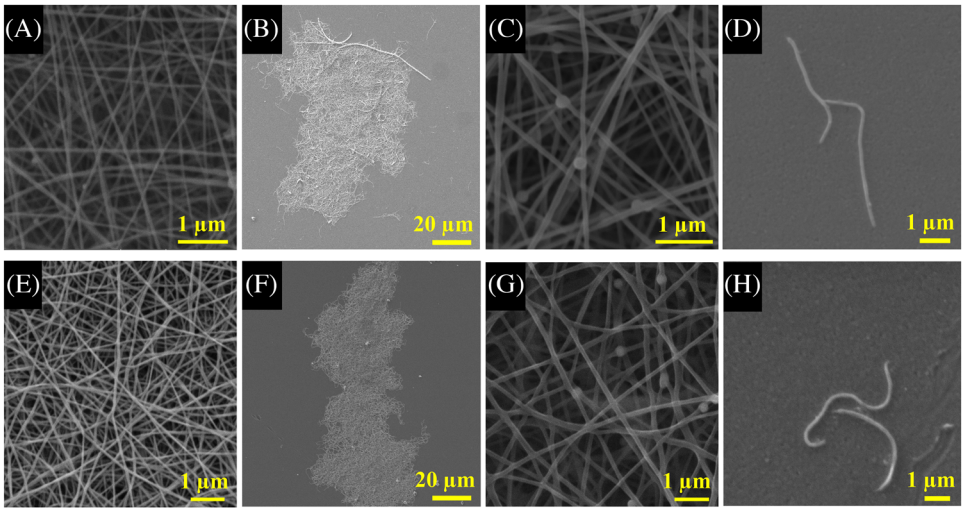

FIGURE 6 Morphological characterization of poly(vinylidene fluoride-trifluoroethylene) (P(VDF-TrFE)) and poly(ε-caprolactone) (PCL) nanofibers with or without SiO_2 nanoparticle integration and subjected to fragmentation. SEM images of electrospun (A-D) P(VDF-TrFE) and (E-H) PCL nanofibers (A, E) without and (C, G) with 20 wt.% SiO_2 nanoparticles before ultrasonication and (B, F), (D-H) their corresponding nanofragments after ultrasonication

80 GPa[26] are considered stiff while PCL represents relatively soft nanofibers having an elastic modulus of approximately 4 GPa.[27] Both types of nanofibers without SiO_2 nanoparticles had an intact membrane after ultrasonication while sonication of nanofibers loaded with 20 wt.% SiO_2 nanoparticles resulted in approximately 4 µm length fragments (Figure 6). Despite the significantly different elastic moduli of P(VDF-TrFE) and PCL nanofibers, both were fragmented once embedded with SiO_2 nanoparticles, indicating that fragmentation is solely dependent on defects generation by the integration of nanoparticles and their subsequent removal. These results suggest

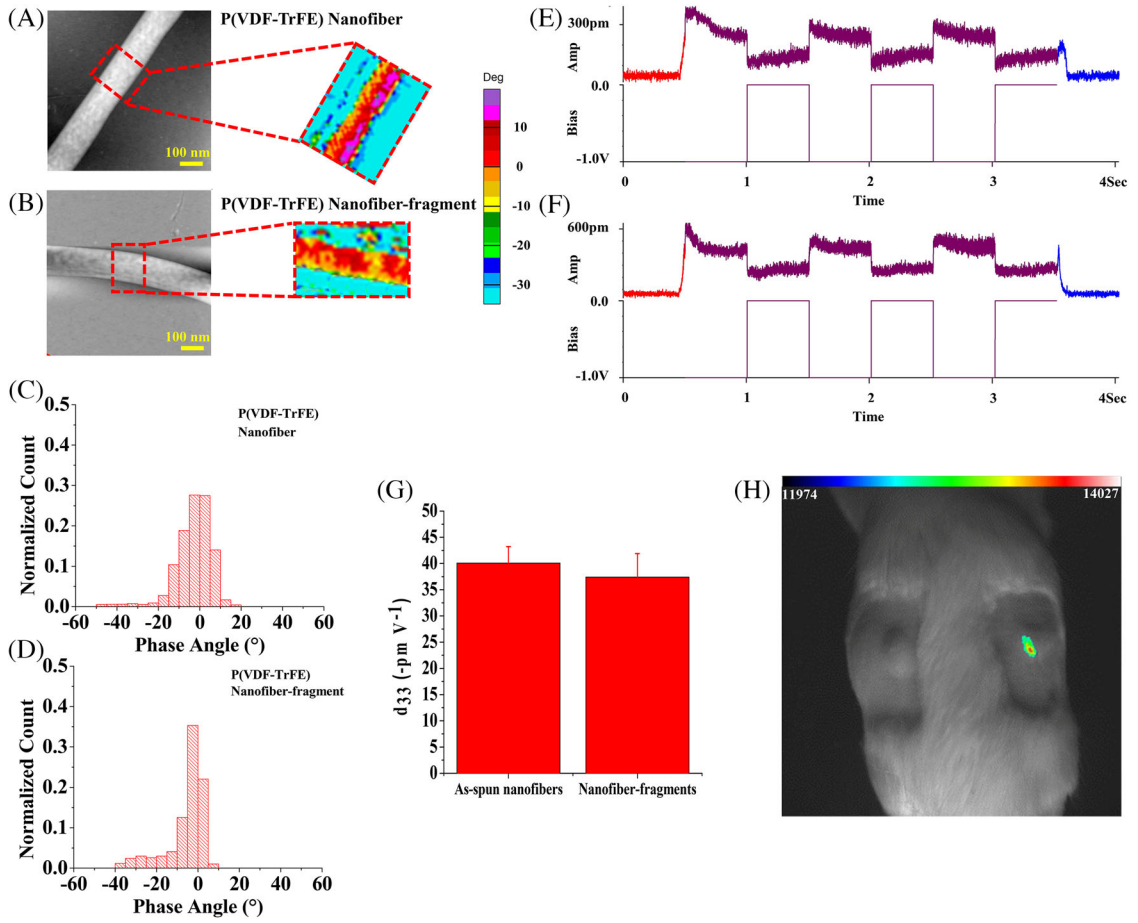

FIGURE 7 Piezoelectric characterization of poly(vinylidene fluoride-trifluoroethylene) (P(VDF-TrFE)) nanofiber-fragments and their bio-application. (A-B) AFM/PFM phase images from (A) as-spun P(VDF-TrFE) nanofiber and (B) nanofiber-fragments. (C-D) Phase angle distribution of (C) as-spun P(VDF-TrFE) nanofibers and (D) nanofiber-fragments with a similar average diameter of 120 nm (n = 3000 measurement points). (E-F) Representative PFM responses from (E) as-spun nanofiber and (F) nanofiber-fragment. (G) Average piezoelectric coefficient, d_{33}, of as-spun nanofibers and nanofiber-fragments with a comparable diameter (117 ± 6 vs. 125 ± 8 nm, respectively). (H) Merged image of optical and photoluminescence imaging demonstrating the injectability of nanofiber-fragments. The left side was injected with pure gelatin methacryloyl (GelMA), a hydrogel (control) while the right side was injected with GelMA containing P(VDF-TrFE) nanofiber-fragments loaded with Vivotag-conjugated poly-L-lysine (PLL), a fluorescent marker

that the method is applicable to a variety of polymers in producing nanofiber-fragments, regardless of their intrinsic mechanical properties.

2.3 | Piezoelectric characterization of the P(VDF-TrFE) nanofiber-fragments and their injectability test

In order to determine any potential changes in material properties after the fragmentation process, that is, piezoelectric dipole alignment, and hence piezoelectric performance, piezoresponse force microscope (PFM) phase imaging was conducted on P(VDF-TrFE) nanofibers or nanofiber-fragments of comparable sizes (Figure 7A-D). Precise nanofiber or nanofiber-fragment location was determined from tapping imaging mode, and the PFM phase imaging was conducted along the length of the nanofiber or nanofiber-fragment (insets) from which phase angle distribution profiles were determined. Phase angle distribution of P(VDF-TrFE) nanofibers (Figure 7C) and nanofiber-fragments (Figure 7D) with average diameters of 120 nm showed a similar distribution. The PFM measurements on individual nanofiber-fragments or nanofibers also revealed that the piezoelectric properties of the nanofibers were preserved after fragmentation, showing that the piezoelectric coefficient, d_{33}, of both the as-spun nanofibers and the nanofiber-fragments was measured to be approximately -40 pm V^{-1} (Figure 7E-G).

To demonstrate the injectability of these PVDF-TrFE nanofiber-fragments for biomedical applications, Vivotag-conjugated poly-L-lysine (PLL) was loaded onto the

nanofiber-fragments. Gelatin methacryloyl (GelMA) hydrogel was used as a carrier for injection as well as to localize the injected nanofiber-fragments in the injection site without dispersion for imaging. Two areas on the lower back of a rat cadaver were shaved; nanofiber-fragments-containing hydrogel was injected into the right side while hydrogel only was injected into the left side to serve as the experimental control. The photoluminescence imaging clearly demonstrated the injectability of nanofiber-fragments (Figure 7H).

3 | CONCLUSION

In summary, we developed a novel method based on colloid electrospinning with sacrificial nanoparticles and ultrasonication to produce polymeric nanofiber-fragments. By creating a beads-on-a-string structure of electrospun nanofibers, we introduced brittle points along the nanofibers that can be fractured under mechanical perturbation. To improve the efficiency of fragmentation, we investigated the effects of silica nanoparticle size and their surface modifications on the integration of the nanoparticles within the polymer matrix. We demonstrated that the nanofiber-fragment length can be precisely controlled by the nanoparticle loading on electrospun nanofibers. Fragmentation of polymer nanofibers with distinct mechanical properties was also performed, demonstrating the broad and facile applicability of this method for various polymers.

4 | EXPERIMENTAL SECTION

Synthesis of SiO_2 nanoparticles: SiO_2 nanoparticles were synthesized based on a previously reported method.[28] Briefly, a solution mixture containing 8 M ethanol (Fisher Scientific, Pittsburgh, PA), 3 M deionized (DI) water, and 14 M ammonium hydroxide (Electron Microscopy Sciences, Hatfield, PA) was prepared. The mole ratio of water/tetraethyl orthosilicate (TEOS) (Sigma-Aldrich, St. Louis, MO) was set at approximately 30, 45, 60, 70, and 120. First, ethanol and water were combined and allowed to mix for 10 minutes in a sonication bath. Then, TEOS was added and the mixture was sonicated for 20 minutes. Ammonium hydroxide was added dropwise to the solution while under sonication to promote the condensation reaction for 60 minutes. The sonication bath temperature was maintained at 35°C. At the end of the reaction, the particles were collected by centrifugation at approximately 12,000 x *g* for 30 minutes using a high-speed centrifuge (Model 5810, Eppendorf, Enfield, CT), washed with ethanol, and dried under a vacuum for 30 minutes. All the steps—centrifugation, washing, and drying—were performed at room temperature.

To calcinate the SiO_2 nanoparticles for enhanced hydrophobicity, the dried nanoparticle agglomerates were crushed into a fine powder with a mortar and pestle for 10 minutes and calcified for 3 hours at 900°C in a heat resistant crucible, using a benchtop furnace (ThermolyneTM, Fisher Scientific). Alternatively, the calcined SiO_2 nanoparticles were silanized to further increase hydrophobicity as described previously.[29] Two hundred milligram of calcined SiO_2 nanoparticles were suspended in 30 mL of toluene (Fisher Scientific) containing 0.5% v/v trimethoxy (octadecyl) silane (OTMS) (Fisher Scientific). The solution was refluxed at 110°C for 20 hours. The surface-modified particles were centrifuged, washed, and dried under a vacuum.

Colloid-electrospinning of P(VDF-TrFE) and PCL nanofibers with SiO_2 nanoparticles: A solution containing 7.0 wt.% poly(vinylidene fluoride-trifluoroethylene) (P(VDF-TrFE)) (70/30 mol%) (Solvay Group, France) dissolved in a 64/36 weight ratio of *N,N*-dimethylformamide (DMF) (Fisher Scientific) and acetone (Fisher Scientific) was utilized to produce a mat composed of P(VDF-TrFE) nanofibers of approximately 120 nm in diameter and embedded with various loadings of SiO_2 nanoparticles. The solution was supplemented with 1.5 wt.% pyridinium formate (PF) buffer (Santa Cruz Biotechnology, Dallas, TX) to enhance electrospinnability. SiO_2 nanoparticles (0, 10, 20, 40, or 60 wt.% with respect to polymer concentration) were added to the solution and sonicated for 1 hour for uniform particle dispersion. Each solution was separately loaded into a 10 mL syringe attached to a 25 G needle. The solution flow rate was controlled at 0.2 mL h^{-1} by a syringe pump (New Era Pump Systems, Inc., Farmingdale, NY). Each solution was electrospun for 2 hours on a 75 × 75 mm^2 aluminum foil collector under optimized conditions of electrospinning distance (20 cm) and applied voltage (approximately −12 kV) (Glassman High Voltage, Inc., High Bridge, NJ) at 23°C with an absolute humidity of 9 g m^{-3}.

Additionally, SiO_2 embedded-nanofibrous membrane composed of poly(ε-caprolactone) (PCL) nanofibers with approximately 100 nm in diameter was synthesized by dissolving 4 wt.% PCL (Sigma-Aldrich) in a 5:1 volume ratio of *N,N,N*-trifluoroethanol (TFE) (Oakwood Products Inc., Estill, SC) and distilled water, 1.5 wt.% PF buffer and 20 wt.% SiO_2 nanoparticles. The solution was electrospun after constant stirring for 2 hours under optimized conditions of electrospinning distance (20 cm), applied voltage (−11 kV), and solution feed rate (0.17 mL h^{-1}) at 23°C with an absolute humidity of approximately 6.0 g m^{-3}.

Morphological and chemical characterization of SiO_2 nanoparticles and SiO_2-embedded P(VDF-TrFE)

nanofibrous membranes: The morphology of the SiO_2 nanoparticles and electrospun SiO_2 embedded-nanofibers was characterized using a VEGA3 scanning electron microscope (SEM) (Tescan Brno, Czech Republic). The SiO_2 particle diameter (n = 30), the nanofiber diameter (n = 60), SiO_2 particle density (n = 50), and inter-particle distance on individual fiber (n = 50) were measured using ImageJ software. Fourier-transform infrared spectroscopy (FTIR) of as-synthesized, calcined, and surface-modified SiO_2 nanoparticles was conducted using Nicolet 6700 FTIR Spectrometer (Fisher Scientific). Each spectrum was obtained by scanning dried powder samples.

Fragmentation of SiO_2 embedded-nanofibrous membranes: Prior to being subjected to mechanical agitation, a 1×1 cm^2 of SiO_2 embedded-P(VDF-TrFE) nanofibrous membrane was subjected to a hot mild alkaline etching treatment to remove the SiO_2 nanoparticles according to a procedure described elsewhere.[30] Briefly, the nanoparticle-embedded nanofibrous membrane was subjected to a 0.2 M concentration of KOH (Fisher Scientific) at a temperature of 70°C for 90 minutes and washed thrice with DI water. Any possibility of dehydrofluorination of the P(VDF-TrFE) membrane, as a consequence of the alkaline treatment, was ruled out by observing no detectable change in the color of the membrane. The SiO_2-removed nanofibrous membrane was immersed in a DI water bath, followed by immersion in a liquid nitrogen bath for 30 minutes each. This series of treatments further increases the brittleness of the P(VDF-TrFE) membrane necessary for effective fragmentation by ultrasonication. Immediately after the liquid nitrogen treatment, the P(VDF-TrFE) nanofibrous membrane was immersed in 2 mL ethanol (Fisher Scientific) in a liquid nitrogen bath. Ultrasonication of the nanofibers was then carried out at a magnitude of 50 W for 6 hours using a sonic dismembrator (Model 50, Fisher Scientific). Centrifugation at 1000 x *g* was used to isolate the unfragmented nanofiber membrane. The supernatant containing the nanofiber-fragments was centrifuged (Centrifuge 5804, Eppendorf, Hamburg, Germany) at 20,000 x g for 30 minutes for collection.

Piezoelectric characterization of P(VDF-TrFE) nanofiber-fragments: The piezoelectric characterization of the P(VDF-TrFE) nanofiber-fragments was carried out similarly as we reported earlier.[16] Briefly, to accurately measure the piezoelectric coefficient, d_{33}, a standard periodically poled lithium niobate (PPLN) with a known piezoelectric coefficient was used to determine a correction factor for all subsequent measurements. Various P(VDF-TrFE) as-spun nanofibers or P(VDF-TrFE) nanofiber-fragments were collected on gold-coated, thermal-oxide silicon substrates and subjected to single-point piezoresponse force microscopy (PFM) on individual nanofibers or nanofiber-fragments. An MFP-3D AFM (Asylum Research, Santa Barbara, CA) was first used in tapping imaging mode to locate an individual nanofiber or nanofiber-fragment. Three to five points were chosen on the scanned nanofiber or nanofiber-fragment and the AFM was switched to PFM mode where single point piezoresponse measurements were conducted. Step voltages from 0 to -3 V were applied across the nanofiber or the nanofiber-fragment via the AFM cantilever (AC240TM, Asylum Research, Santa Barbara, CA). A value of d_{33} was calculated by,

$$d_{33} = \frac{A}{VQ} f \tag{1}$$

where A is the amplitude response of the nanofiber or nanofiber-fragment in response to an applied voltage (V), Q is the quality factor of the AFM cantilever, and f is the correctional factor derived from the PPLN standard measurement. Alternatively, to determine the effects of the fragmentation process on polymer chain/dipole alignment, and in turn, piezoelectric performance, PFM phase imaging was conducted on P(VDF-TrFE) as-spun nanofibers or P(VDF-TrFE) nanofiber-fragments with 120 ± 10 nm average fiber diameter for both as-spun nanofibers and nanofiber-fragments. The precise nanofiber or nanofiber-fragment location was determined from tapping imaging mode, and the PFM phase imaging was conducted along the length of the nanofiber or nanofiber-fragment from which phase angle distribution profiles were determined. It should be noted that due to the pyramidal geometry of the AFM tip, in-plane scanning causes a common imaging artifact in which the nanofiber or nanofiber-fragment appears to be wider than the actual nanofiber or nanofiber-fragment diameter (height) in the 3D scanned image.[31] Therefore, the out-of-plane height value was used to determine the actual nanofiber or nanofiber-fragment diameter during the PFM measurements.

Injectability test of P(VDF-TrFE) nanofiber-fragments: To demonstrate the applicability of nanofiber-fragments for drug delivery applications, their injectability was tested in an animal model. Poly-L-lysine (PLL) conjugated with a photoluminescence fluorochrome was used as a model drug in this study. Briefly, poly-L-lysine hydrobromide (30-70 kDa, Sigma) was dissolved in 50 mM sodium borate buffer (Fisher Scientific) at pH 8.5. Vivotag-645 fluorochrome (PerkinElmer, Waltham, MA) was added into the mixture for the final concentration of PLL and Vivotag-645 at 2 and 48 nM, respectively. The reaction was allowed to proceed under stirring for 6 hours at room temperature. The nanofiber-fragment-containing supernatant from the ultrasonication step was centrifuged at 20,000 x *g* for 30 minutes and the pellet containing the nanofiber-fragments was washed once with 1x PBS, prior to drug loading. The washing of the pellet was carried out by mixing it with 1 mL of 1x PBS, followed by

centrifugation at 20,000 x *g* for 30 minutes, and then discarding the supernatant. After exposing the washed sample to the Vivotag-conjugated PLL solution overnight on a shaker plate, the solution was centrifuged at 20,000 x g for 30 minutes and the pellet was collected. Any loosely bound or unbound dye was removed from the nanofiber-fragments by the aforementioned PBS washing process.

The solution for the injection experiment was prepared by mixing the drug-loaded nanofiber-fragments with 100 μL of gelatin methacryloyl (GelMA) solution, synthesized as described elsewhere.[32] Pure 100 μL of GelMA without the nanofiber-fragments was used as a control. A rat cadaver was used to test the injectability of the nanofiber-fragments. Two subcutaneous areas, one on the right side and the other on the left side, on the caudal end of the dorsal side were shaved for the injection experiment. The area on the right side was injected with hydrogel solution containing the drug-loaded nanofiber-fragments, while the area on the left side was injected with hydrogel without the nanofiber-fragments. The injected hydrogels were photo-crosslinked by brief visible light exposure. The photoluminescence of the model drug in the rat body was visualized in a luminescence dark box with a PIXIS 1024B camera (filter: 690 ± 50 nm). WinView software was used to visualize photoluminescence emitted from the dye in the nanofiber-fragment-containing hydrogel.

ACKNOWLEDGMENTS

This work was supported by the National Science Foundation (CBET-1805975), the Creative Materials Discovery Program through the National Research Foundation of Korea funded by the Ministry of Science and ICT (2018M3D1A1057844), and UC Riverside and Korea Institute of Materials Science (Research Program PNK7280) through UC-KIMS Center for Innovative Materials for Energy and Environment.

DATA AVAILABILITY STATEMENT

Research data are not shared.

REFERENCES

1. L. Shang, K. Nienhaus, G. U. Nienhaus, *J. Nanobiotechnol.* **2014**, *12*, 1.
2. S. Wang, J. G. Li, Z. X. Zhou, S. Zhou, Z. Q. Hu, *Molecules* **2019**, *24*(1), 75.
3. M. W. Tibbitt, C. B. Rodell, J. A. Burdick, K. S. Anseth, *P. Natl. Acad. Sci. USA* **2015**, *112*, 14444.
4. K. E. Uhrich, S. M. Cannizzaro, R. S. Langer, K. M. Shakesheff, *Chem. Rev.* **1999**, *99*, 3181.
5. N. Angelova, D. Hunkeler, *Trends Biotechnol.* **1999**, *17*, 409.
6. J. Tsung, D. J. Burgess, in *Fundamentals and Applications of Controlled Release Drug Delivery*, (Eds: J. Siepmann, R. A. Siegel, M. J. Rathbone), Springer US: Boston, MA, US **2012**, 107.
7. D. A. Bedoya, F. N. Figueroa, M. A. Macchione, M. C. Strumia, in *Advanced Biopolymeric Systems for Drug Delivery*, (Eds: A. K. Nayak, M. S. Hasnain), Springer International Publishing: Cham, **2020**, 115.
8. T. Jariwala, G. Ico, Y. Tai, H. Park, N.V. Myung, J. Nam, *ACS Applied Bio Materials* **2021**, *4*, 3706.
9. Y. N. Zhang, W. Poon, A. J. Tavares, I. D. McGilvray, W. C. W. Chan, *J. Control Release* **2016**, *240*, 332.
10. K. Ogawara, M. Yoshida, K. Higaki, T. Kimura, K. Shiraishi, M. Nishikawa, Y. Takakura, M. Hashida, *J. Control Release* **1999**, *59*, 15.
11. R. Dash, A. J. Ragauskas, *Rsc. Adv.* **2012**, *2*, 3403.
12. A. Hasan, G. Waibhaw, S. Tiwari, K. Dharmalingam, I. Shukla, L. M. Pandey, *J. Biomed. Mater. Res. A* **2017**, *105*, 2391.
13. M. Suzuki, R. Kita, H. Hara, K. Hamachi, K. Nagai, K. Nakajima, K. Kimura, *J. Electrochem. Soc.* **2010**, *157*, K34.
14. J. Kim, M. Jun, S. Choi, J. Jo, K. Lee, *Nanoscale* **2019**, *11*, 20392.
15. S. Ramakrishna, K. Fujihara, W. E. Teo, T. Yong, Z. W. Ma, R. Ramaseshan, *Mater. Today* **2006**, *9*, 40.
16. G. Ico, A. Myung, B. S. Kim, N. V. Myung, J. Nam, *Nanoscale* **2018**, *10*, 2894.
17. S. Kim, G. Ico, Y. Bai, S. Yang, J. H. Lee, Y. Yin, N. V. Myung, J. Nam, *Nanoscale* **2019**, *11*, 20527.
18. R. S. Bhattarai, R. D. Bachu, S. H. S. Boddu, S. Bhaduri, *Pharmaceutics* **2018**, *11*(1), 5.
19. K. Fujihara, A. Kumar, R. Jose, S. Ramakrishna, S. Uchida, *Nanotechnology* **2007**, *18*(36), 365709.
20. S. H. Jiang, G. G. Duan, J. Schobel, S. Agarwal, A. Greiner, *Compos. Sci. Technol.* **2013**, *88*, 57.
21. M. Sawawi, T. Y. Wang, D. R. Nisbet, G. P. Simon, *Polymer* **2013**, *54*, 4237.
22. F. Deuber, S. Mousavi, M. Hofer, C. Adlhart, *ChemistrySelect* **2016**, *1*, 5595.
23. S. C. Feifel, F. Lisdat, *J Nanobiotechnol* **2011**, *9*, 59.
24. Y. Z. Chen, Z. P. Zhang, J. Yu, Z. X. Guo, *J. Polym. Sci. B Polym. Phys.* **2009**, *47*(12), 1211.
25. X. Y. Li, W. C. Chen, Q. R. Qian, H. T. Huang, Y. M. Chen, Z. Q. Wang, Q. H. Chen, J. Yang, J. Li, Y. W. Mai, *Adv. Energy Mater.* **2021**, *11*, 2000845.
26. G. Ico, A. Showalter, W. Bosze, S. C. Gott, B. S. Kim, M. P. Rao, N. V. Myung, J. Nam, *J. Mater. Chem. A* **2016**, *4*, 2293.
27. F. Croisier, A. S. Duwez, C. Jerome, A. F. Leonard, K. O. van der Werf, P. J. Dijkstra, M. L. Bennink, *Acta Biomater.* **2012**, *8*, 218.
28. K. S. Rao, K. El-Hami, T. Kodaki, K. Matsushige, K. Makino, *J. Colloid Interf. Sci.* **2005**, *289*(1), 125.
29. Y. T. Niu, M. H. Yu, A. Meka, Y. Liu, J. Zhang, Y. N. Yang, C. Z. Yu, *J. Mater. Chem. B* **2016**, *4*, 212.
30. N. A. Samsure, N. A. Hashim, N. M. N. Sulaiman, C. Y. Chee, *Rsc Adv.* **2016**, *6*, 22153.
31. J. J. Schneider, J. Engstler, S. Franzka, K. Hofmann, B. Albert, J. Ensling, P. Gutlich, P. Hildebrandt, S. Dopner, W. Pfleging, B. Gunther, G. Muller, *Chemistry* **2001**, *7*, 2888.
32. J. W. Nichol, S. T. Koshy, H. Bae, C. M. Hwang, S. Yamanlar, A. Khademhosseini, *Biomaterials* **2010**, *31*, 5536.

How to cite this article: A. Banerjee, T. Jariwala, S. Kim, Y. Tai, S. Chiang, H. Park, N. V. Myung, J. Nam, *Nano Select* **2021**, 1.
https://doi.org/10.1002/nano.202100194